Variation Regularity and Measurement of Zero-Sequence Inductance of Fractional Slot Concentrated Winding PMSMs

Zhu, Zichong; Deng, Jun; Dou, Xun; Mei, Lei; Huang, Yunkai; Dong, Jianning

Variation Regularity and Measurement of Zero-Sequence Inductance of Fractional Slot Concentrated Winding PMSMs

Zichong Zhu [ID], Jun Deng, Xun Dou [ID], *Member, IEEE*, Lei Mei, *Member, IEEE*, Yunkai Huang [ID], and Jianning Dong [ID], *Member, IEEE*

Abstract—The zero-sequence inductance is a vital parameter for the performance analysis of permanent magnet machines, especially under faulty conditions or in open-winding machines. This paper focuses on the zero-sequence inductance calculation of fractional slot concentrated winding permanent magnet synchronous machines (FSCW-PMSMs), and reveals the variation regularity of this kind of inductance and its various components against pole/slot combinations, using the winding function and finite element methods. Moreover, based on the analysis of 36-slot FSCW-PMSMs with different pole numbers, the dependency of each inductance component on the pole/slot combination is discussed in detail. To validate the regularities, experimental measurements of zero-sequence inductance are implemented in the prototype of the 36-slot stator. It is found that the regularities are independent of specific slot or pole numbers, which provide guidelines for optimum pole/slot combination selection, to mitigate the problems caused by zero-sequence current.

Index Terms—Fractional slot concentrated winding, inductance measurement, permanent magnet machine, winding function, zero-sequence inductance.

I. INTRODUCTION

OWING to their high torque density, high efficiency, and superior fault tolerance, fractional slot concentrated winding permanent magnet synchronous machines (FSCW-PMSMs) are attractive in many fields, such as servo, wind power generation, and wheel-hub traction [1]–[3]. Fractional slot concentrated winding machines (FSCWMs) feature short end winding, large pole/slot numbers, and thin stator/rotor yokes, and thus a torque

(a) 3-phase winding with a neutral ground (b) Single-phase short circuit

(c) 3-phase machine with open windings

Fig. 1.   Scenarios where zero-sequence current exists.

density higher than that of integer slot distributed winding machines (ISDWMs) is usually produced.

Due to a fractional number of slots per pole per phase q, FSCWMs have vast feasible pole/slot combinations [4], especially when the slot and pole numbers are large. Moreover, for certain combination, more than one winding layouts (phase coil arrangement) exist [5]. As a consequence, selecting the optimum pole/slot combination for FSCWMs is complicated. Simply multiplying the unit combination, such as 8P9S (8-poles 9-slots FSCWM with two-layer windings) and 10P12S, may not result in the most competitive solution.

Therefore, comparisons of key performance indicators for different pole/slot combinations are essential at the initial design stage, e.g., torque density [6], electromagnetic loss reduction [7], unbalanced magnetic pull [8], toque ripple [9], new winding scheme [10], fault-tolerant ability [11] *et al*. These researches evaluate and compare performances from the 3-phase balanced magnetic field point of view, assuming there is no zero-sequence current. Whereas, in the cases of the faulty condition [12], open-winding machine [13] or star-connected winding scheme with grounded neutral point [14], as shown in Fig. 1, the zero-sequence current exists and related issues arise, such as additional electromagnetic loss, torque ripples [14], and low control accuracy [15].

A large zero-sequence (ZS) inductance L_0 helps to reduce zero-sequence current [15] or improves the performance of the fault-tolerant operation. On the other hand, accurate calculation of L_0 is essential for the steady/dynamic simulation, controller design, and fault-handling control strategy, e.g., common-mode voltage rejection. Some researchers investigated the calculation

of L_0 [16], and its influencing factors [17], yet the variation of L_0 against pole/slot combinations, accurate separation of various components of L_0, and relevant experimental validations are absent.

The purpose of this paper is to derive the general variation regularity of L_0 and its components for FSCWMs with various pole/slot combinations, which contributes to determining the optimum design space of pole/slot numbers, solving the issues caused by zero-sequence current, and improving the fault-tolerant ability at the machine design stage, instead of resorting to the control side [13], [18], [19]. In addition, this paper presents the measurement of zero-sequence inductance under various conditions, to validate the regularities by experimental results.

Specifically, 36-slot FSCW-PMSMs with different pole numbers are exampled to demonstrate the variation regularities of ZS inductance, using analytical winding function theory and finite element method (FEM). The contents of this paper are arranged as: in Section II, the magnetomotive force (MMF) of ISDWMs and FSCWMs are compared, to discuss the source of ZS inductance. Based on the winding function theory, the air-gap and intrinsic ZS inductances are analytically calculated and compared. Section III introduces the source of the stray ZS inductance and explains the reason for the low accuracy of analytical models. Meanwhile, FEM is used to calculate each component of ZS inductance, to further reveal the variation regularities. Then, the prototype of the 36-slot FSCWM and experimental setups are introduced, where ZS inductances are measured to validate the variation regularities.

Owing to less rotor flux leakage and higher torque density, a surface-mounted permanent magnet (SPM) rotor is more often used in FSCWMs. Meanwhile, as was pointed out in [20], [21], the double-layer winding compromises the spatial MMF harmonics, manufacturing complexity, and fault-tolerant ability, compared to single-layer and multi-layer windings, thus are preferred in FSCWMs. Therefore, this paper deals with FSCWMs with SPM rotors and double-layer windings.

II. CALCULATION OF INTRINSIC ZS INDUCTANCE IN ISDWMS AND FSCWMS

This section discusses the source and calculation of the intrinsic ZS inductance L_{i0} and compares its quantity in ISDWMs and FSCWMs.

A. Winding Layouts and MMFs of ISDWM and FSCWM

Taking 8-poles 48-slots ISDWM (8P48S) and 8-poles 9-slots FSCWM (8P9S) as examples, two-layer winding layouts of them are shown in Fig. 2. When ignoring the slotting and saturation effect, the single-phase and synthesized 3-phase armature MMFs with purely sine current fed into windings are illustrated in Fig. 3, where each MMF is normalized to the ampere-turns of a coil.

It can be seen from Fig. 3, due to a large number of slots per pole per phase ($q = 2$), the winding layout of 8P48S resembles a sinusoidal distribution. As a consequence, the single-phase and synthesized 3-phase MMFs are approximately sinusoidal waves, and spatial harmonics have high orders but small amplitudes, compared to the fundamental. Nevertheless, MMF of 8P9S is

(a) 8P48S (1/4 part)

(b) 8P9S
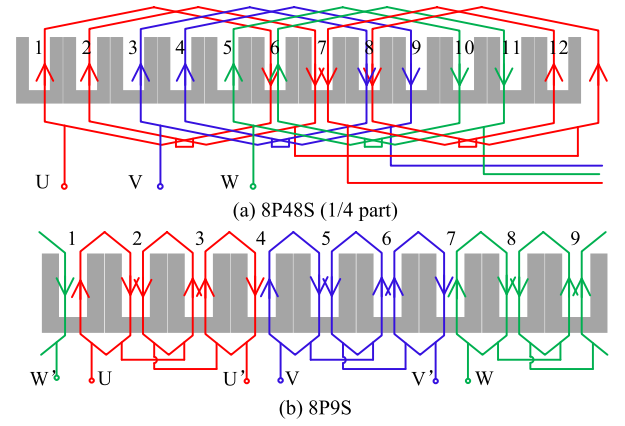
Fig. 2.　Winding layouts of 8P48S and 8P9S.

(a) 8P48S

(b) 8P9S
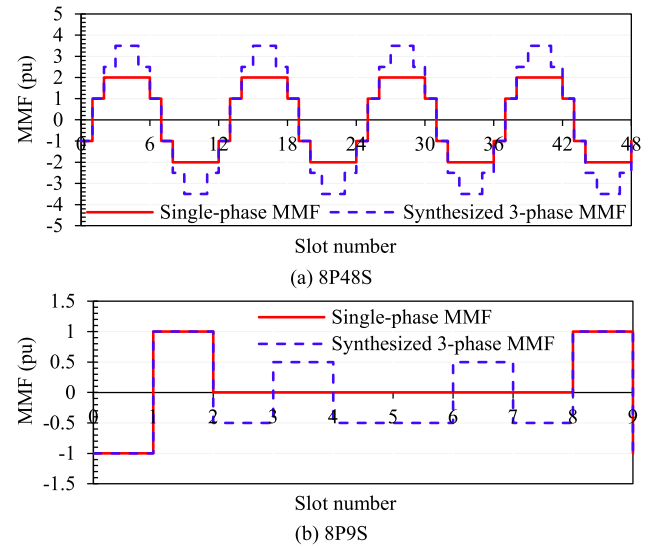
Fig. 3.　The armature MMFs of 8P48S and 8P9S.

far from sinusoidal, the spatial harmonics have orders close to and amplitudes comparable to that of the fundamental. Some of these harmonics are canceled in the synthesized MMF, and will not affect the performances of a 3-phase balanced system. But for the scenarios presented in Fig. 1, the zero-sequence current appears, and these canceled harmonics influence the machine's performance significantly.

B. Intrinsic ZS Inductance

The armature MMF produced by U-phase winding relates to its winding function $N_u(\theta)$, which has even symmetry and can be decomposed to the Fourier series as

$$
\begin{aligned}
N_u(\theta) &= \frac{2T_{ph}k_{w1}}{\pi}\cos(\theta + \varphi_1) + \frac{2T_{ph}k_{w2}}{2\pi}\cos(2\theta + \varphi_2) \\
&\quad + \frac{2T_{ph}k_{w3}}{3\pi}\cos(3\theta + \varphi_3) + \ldots \\
&= \frac{2T_{ph}}{\pi}\sum_{\nu=1,2,3,\ldots}^{\infty}\frac{k_{w\nu}}{\nu}\cos(\nu\theta + \varphi_\nu),
\end{aligned}\tag{1}
$$
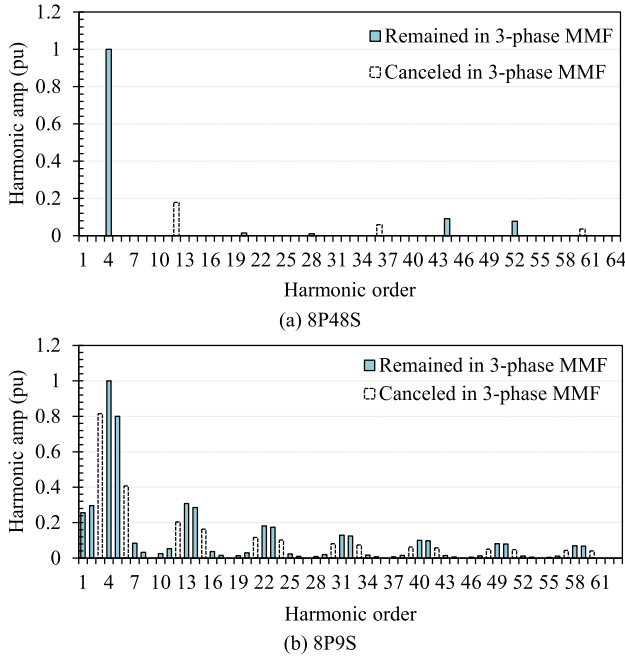
Fig. 4. Spectra of the single-phase MMF of 8P48S and 8P9S.

where $k_{w\nu}$ and φ_ν are the winding factor and initial phase of the νth harmonic respectively. φ_ν can only be π or 0 due to the even symmetry of $N_u(\theta)$. T_{ph} is the total turns in series of a phase winding. It is noteworthy that, θ is measured in mechanical reference here. With this definition, the 1st harmonic has a period of 2π mechanical radians, and not necessarily be the fundamental. For example, in 8P9S, the 1st harmonic has one pole pair along the circumference, yet the fundamental has 4 pole pairs and is the 4th harmonic.

When all phase windings are excited by a 3-phase sinusoidal current (3), the synthesized winding function $N_{uvw}(\theta)$ are

$$N_{uvw}(\theta) = \frac{3T_{ph}k_{w1}}{\pi}\cos(\theta + \varphi_1) + \frac{3T_{ph}k_{w2}}{2\pi}\cos(2\theta + \varphi_2)$$

$$+ \frac{3T_{ph}k_{w4}}{4\pi}\cos(4\theta + \varphi_4) + \dots$$

$$= \frac{3T_{ph}}{\pi}\sum_{\substack{\nu=1,2,3,\dots \\ \nu \neq 3kn, k=1,2,3,\dots}}^{\infty} \frac{k_{wv}}{\nu}\cos(\nu\theta + \varphi_\nu). \quad (2)$$

$$\begin{cases} i_u(t) = I_m\cos(\omega t) \\ i_v(t) = I_m\cos(\omega t - 2\pi/3) \\ i_w(t) = I_m\cos(\omega t + 2\pi/3) \end{cases} \quad (3)$$

In (2), n is the number of unit motors, e.g., 8P48S consists of 4 unit motors, and $n = 4$. Whereas, 8P9S itself is a unit motor, thus $n = 1$.

It can be seen in (2), due to the symmetrical distribution of 3-phase windings, harmonics with order equal $3kn$ are canceled in $N_{uvw}(\theta)$. Fig. 4 gives the spectra of the single-phase MMF of 8P48S and 8P9S (presents up to the 60th harmonic), and the harmonics canceled in synthesized 3-phase MMFs are marked with a dashed frame. In addition, since the 3-phase windings are

arranged by shifting $\pm 2\pi/3$ radians to each other, the amplitude of the harmonics remained in synthesized MMF is 3/2 times larger, considering the mutual coupling factor 1/2 between either two phases.

However, when all 3-phase windings are supplied by zero-sequence current i_0 that has identical amplitude, frequency, and initial phase in each phase winding, as in (4),

$$i_u(t) = i_v(t) = i_w(t) = i_0(t) = I_0\cos(\omega_0 t) \quad (4)$$

MMF of each phase $f_u(t,\theta), f_v(t,\theta)$, and $f_w(t,\theta)$ can be written as

$$\begin{cases} f_u(t,\theta) = N_u(\theta)i_u(t) = N_u(\theta)i_0(t) \\ \qquad = \frac{2T_{ph}I_0}{\pi}\sum_{\nu=1,2,3,\dots}^{\infty}\frac{k_{w\nu}}{\nu}\cos(\nu\theta)\cos(\omega_0 t) \\ f_v(t,\theta) = N_v(\theta)i_v(t) = N_v(\theta)i_0(t) \\ \qquad = \frac{2T_{ph}I_0}{\pi}\sum_{\nu=1,2,3,\dots}^{\infty}\frac{k_{w\nu}}{\nu}\cos\left(\nu\theta - \frac{2\nu\pi}{3}\right)\cos(\omega_0 t) \\ f_w(t,\theta) = N_w(\theta)i_w(t) = N_w(\theta)i_0(t) \\ \qquad = \frac{2T_{ph}I_0}{\pi}\sum_{\nu=1,2,3,\dots}^{\infty}\frac{k_{w\nu}}{\nu}\cos\left(\nu\theta + \frac{2\nu\pi}{3}\right)\cos(\omega_0 t) \end{cases} \quad (5)$$

The synthesized 3-phase MMF $f_{uvw}(t, \theta)$, is therefore given by

$$f_{uvw}(t,\theta) = \frac{6T_{ph}I_0}{\pi}\sum_{\nu=3kn, k=1,2,3,\dots}^{\infty}\frac{k_{w\nu}}{\nu}\cos(\nu\theta)\cos(\omega_0 t) \quad (6)$$

$f_{uvw}(t, \theta)$ consists of the harmonics with orders equal $3kn$ that are canceled in (2), these harmonics are usually referred to as the zero-sequence harmonics.

The air-gap inductance L_g when windings are excited by a 3-phase symmetrical current is calculated using $N_u(\theta)$ and $N_{uvw}(\theta)$, as in (7), where the self- and mutual components of L_g are counted simultaneously. In (7), δ is the equivalent air gap length, r_{si} and L_{stk} are the inner radius and axial length of the stator lamination.

$$L_g = \frac{\mu_0 r_{si}L_{stk}}{\delta}\int_0^{2\pi}N_u(\theta)N_{uvw}(\theta)\,d\theta$$

$$= \frac{6\mu_0 r_{si}L_{stk}T_{ph}^2}{\pi\delta}\sum_{\substack{\nu=1,2,3,\dots \\ \nu \neq 3kn, k=1,2,3,\dots}}^{\infty}\frac{k_{w\nu}^2}{\nu^2} \quad (7)$$

Similar to L_g, using U-phase and 3-phase winding functions $N_{u0}(\theta)$, $N_{uvw0}(\theta)$ when $i_0(t)$ is supplied, the ZS inductance L_{i0} is written as

$$L_{i0} = \frac{\mu_0 r_{si}L_{stk}}{\delta}\int_0^{2\pi}N_{u0}(\theta)N_{uvw0}(\theta)\,d\theta$$

$$= \frac{12\mu_0 r_{si}L_{stk}T_{ph}^2}{\pi\delta}\sum_{\nu=3kn, k=1,2,3,\dots}^{\infty}\frac{k_{w\nu}^2}{\nu^2} \quad (8)$$

L_{i0} in (8) takes the air-gap flux into account and is usually referred to as the intrinsic ZS inductance [16].
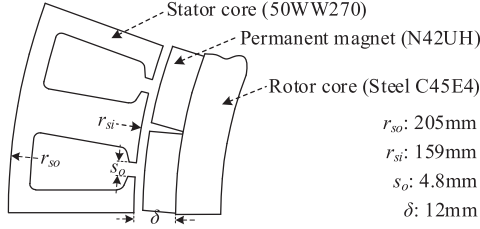
Fig. 5.   Partial cross-section of 36-slot FSCWMs and main geometry sizes.

As shown in Fig. 4(a), the high-order MMF harmonics of ISDWM have small amplitudes, especially for the ones constituting L_{i0} ($\nu = 3kn$). As a consequence, L_{i0} is negligible compared to L_g in ISDWMs. However, this is not the case for FSCWMs, whose MMFs are far from sinusoidal, and contain rich harmonics. Moreover, some of these harmonics have amplitudes comparable to the fundamental, particularly the sub-harmonics with $\nu < p$. As a result, L_{i0} of FSCWMs is of the same order of magnitude as L_g. For example, the ratio between L_{i0} and L_g is referred to as the zero-sequence ratio σ, which are 0.073 and 0.892 (counting harmonics with $\nu < 100$) for 8P48S and 8P9S respectively.

From (7) and (8), σ is calculated with ν and $k_{w\nu}$ that relate to the machine's pole/slot combination and winding layout, but is independent of specific winding parameters and geometry sizes, as in (9).

$$\sigma = \frac{L_{i0}}{L_g} = 2 \sum_{\nu=3kn,k=1,2,3,...}^{\infty} \frac{k_{w\nu}^2}{\nu^2} \Bigg/ \sum_{\substack{\nu=1,2,3,... \\ \nu \neq 3kn,k=1,2,3,...}}^{\infty} \frac{k_{w\nu}^2}{\nu^2} \tag{9}$$

Unfortunately, the winding layout and uniform winding function expression for FSCWMs cannot be solely determined from the pole number $2p$, slot number z, and coil pitch, like that in ISDWMs, because of the fractional number of q and fixed coil pitch. Usually, the winding layout of FSCWMs are organized using the star-of-slot theory [22] or systematic method [5], which both seek a high fundamental winding factor k_{wp} and thus large torque density. The following sections explore the variation trend of inductance against pole/slot combinations, particularly the ZS inductance.

III. VARIATION REGULARITIES OF INTRINSIC ZS INDUCTANCE

A. Machine Models

As mentioned above, FSCWMs have abundant pole/slot combinations when with a large number of slots and poles, it is hard and unfair to perform comparisons with different winding parameters and geometry sizes. Therefore, in this paper, 36-slot FSCWs with different pole numbers, are investigated to clarify the inductance variation regularities. The main dimensions, materials, and winding parameters are given in Fig. 5 and Table I. These 36-slot FSCWMs have identical rated power of 55 kW and operation speed of 525r/min. The current density is designed constant for all machines at 9.56A/mm². Since these machines have identical speed but different pole numbers, their fundamental frequencies vary in the range of 105~210 Hz.

TABLE I
DESIGN PARAMETERS OF ANALYZED MACHINES

Machine	$2p$	z	T_c	a	T_{ph}	k_{wp}	q
24P36S	24					0.866	1/2
26P36S	26					0.867	6/13
28P36S	28					0.902	6/14
30P36S	30					0.933	2/5
32P36S	32					0.945	3/8
34P36S	34	36	8	1	96	0.953	6/17
38P36S	38					0.953	6/19
40P36S	40					0.945	3/10
42P36S	42					0.933	2/7
44P36S	44					0.902	3/11
46P36S	46					0.867	6/23
48P36S	48					0.866	1/4

The winding layout of each machine is determined using the systematic method [5], as shown in Fig. 6. The winding layout of machines that have $2p > z$ are not presented in Fig. 6, since their winding layouts are identical to that of machines with $2p < z$. For example, 24P36S and 48P36S share the same winding layout, MMF spectrum, and thus have identical inductances. But it deserves to note that, the phase sequence and fundamental harmonic order of these two combinations are different since 24P36S and 48P36S respectively use the 12th and 24th harmonics as the fundamental.

The minimal and maximal pole numbers analyzed are 24 and 48, to guarantee the fundamental winding factor k_{wp} larger than 0.866. For fair comparisons, except for the same stator and rotor geometries, the number of turns per coil T_c and parallel paths of each phase winding a is designed identical for all machines, and then T_{ph} is constant when $2p$ changes.

B. Variation of Intrinsic ZS Inductance Against Pole Numbers

According to winding layouts in Fig. 6, the winding function of each machine is obtained, then L_g and L_{i0} are calculated using (7) and (8), respectively. Fig. 7 shows the variation of L_g and L_{i0} (counting up to the 200th harmonic) against pole numbers. It can be seen that L_g are approximately constant for all machines, indicating that the winding layout does not influence the flux-establishing ability of MMFs.

A similar variation trend is observed for L_{i0}, though it intrinsically relates to the harmonic distribution of MMF. Since the total zero-sequence harmonic of MMF changes minorly when pole number changes, as presented in Fig. 8(b)–(f), L_{i0} is nearly constant for all combinations and approximates L_g. However, 24P36S and 48P36S are exceptions, these two combinations evolved from the 2P3S and 4P3S units, and their MMFs do not contain zero-sequence harmonics, as shown in Fig. 8(a). As a result, these two machines are not competitive when trying to suppress the zero-sequence current by a large L_{i0}.

IV. STRAY ZS INDUCTANCE

A. Calculation and Variation of Stray ZS Inductance

Except for the air-gap flux, flux leakage in different parts of the stator is non-negligible, especially in FSCWMs that have smaller coil pitches (commonly equal to 1) than ISDWMs. Stator flux
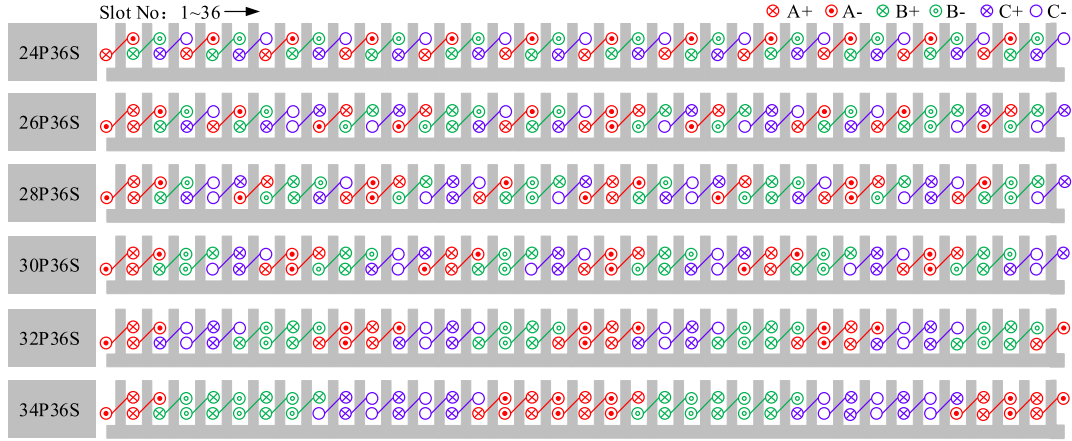
Fig. 6. Winding layouts of 24P36S, 26P36S, 28P36S, 30P36S, 32P36S, and 34P36S.
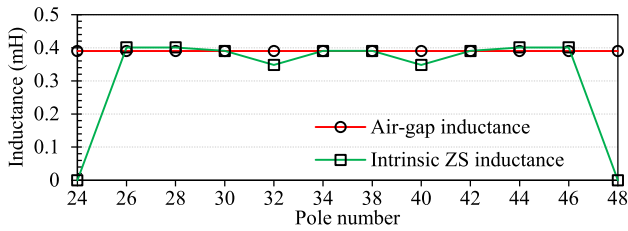

Fig. 7. Inductances calculated using the winding function method.

leakage appears in the slot, tooth tip, and end winding regions. When feeding the zero-sequence current into 3-phase windings, the stator flux leakage also produces ZS inductance, which is usually referred to as the stray ZS inductance L_{s0}.

Some analytical models are proposed in the literature [23], [24], to calculate the stator flux leakage and corresponding leakage inductance L_σ. But they all ignore the effect of winding layout and the mutual component of L_σ, causing a poor prediction accuracy. Therefore, FEM is used here to calculate the stator flux leakage and L_{s0}, as in (10), where ψ_{s0} is the zero-sequence flux linkage.

$$L_{s0} = \frac{\psi_{s0}}{i_0} \tag{10}$$

ψ_{s0} is calculated by the line integral of magnetic potential A, and in 2D-FEM, ψ_{s0} is simplified as

$$\psi_{s0} = T_{ph}L_{stk}\left[\frac{1}{S_1}\iint_{S_1} A_1 ds - \frac{1}{S_2}\iint_{S_2} A_2 ds\right]. \tag{11}$$

A_1 and A_2 are the magnetic potentials in winding cross-Sections S_1 and S_2 in the 2D-FEM plane, where positive and negative currents are flowing into the plane respectively.

Owing to the short and non-overlapping structure of the end winding, as shown in Fig. 9, the end-winding inductance L_{ew} of FSCWM is relatively small. For example, using the method in [25], [26] that differentiates 3D-FEM (the geometry and sizes of the end winding are derived from the stator prototype) and 2D-FEM calculated results, L_{ew} of the 36-slot stator is 0.02mH and only 1.28% of the synchronous inductance. In addition, L_{ew}

is almost constant for 24P36S~48P36S, i.e., independent of the pole numbers and winding layouts. Therefore, L_{ew} is neglected in the calculation of L_{s0} using 2D-FEM.

To separate the stator flux leakage that appears in the slot, tooth tip, and end winding regions from the total armature flux, symmetry boundary conditions are imposed on the inner surfaces of the stator core [26], [27], as shown in Fig. 10. When zero-sequence current is supplied, the winding armature flux can be divided into two components. One is the stator flux leakage that relates to the stray ZS inductance L_{s0}, and the other one enters the air gap, corresponding to the intrinsic ZS inductance L_{i0}. The symmetry boundary conditions imposed in the FEM model hinder armature flux from entering the air gap, and the MMF produces only stator flux leakage. In this case, the winding flux linkage is solely sourced from the stator flux leakage, and the calculated ZS inductance is therefore L_{s0}. It deserves to mention that, to consider potential local magnetic saturation, the permeability of the stator core is set to that derived from the case that calculates the total ZS inductance, by the frozen permeability method.

In addition, to increase the slot fill factor, a segmented stator structure is used, as shown in Fig. 9, where coils are wound on the stator teeth. According to [15], [17], the position of coil sides in a slot strongly influences L_σ and L_{s0}. To improve accuracy, the two coil sides in the FEM model are located adjacent to the tooth, which resembles that in the prototype. Feeding 3-phase sinusoidal current (3) or zero-sequence current (4), L_σ and L_{s0} are respectively calculated.

Fig. 11 shows the calculated stator leakage inductance L_σ and phase inductance L_p, where L_p is calculated using 2D-FEM by disabling permanent magnets. It can be seen that when $2p < z$, both L_p and L_σ increase when more poles are used. However, when $2p > z$, the variation trend reverses. In other words, combinations that have pole numbers close to the slot number (close pole-slot combinations), e.g., 34P36S and 38P36S have the maximal L_σ and L_p. In addition, it can also be seen from Fig. 11 that, in FSCWMs with SPM rotor L_p is dominated by L_σ, since in all machines, L_σ exceeds 60% of L_p.
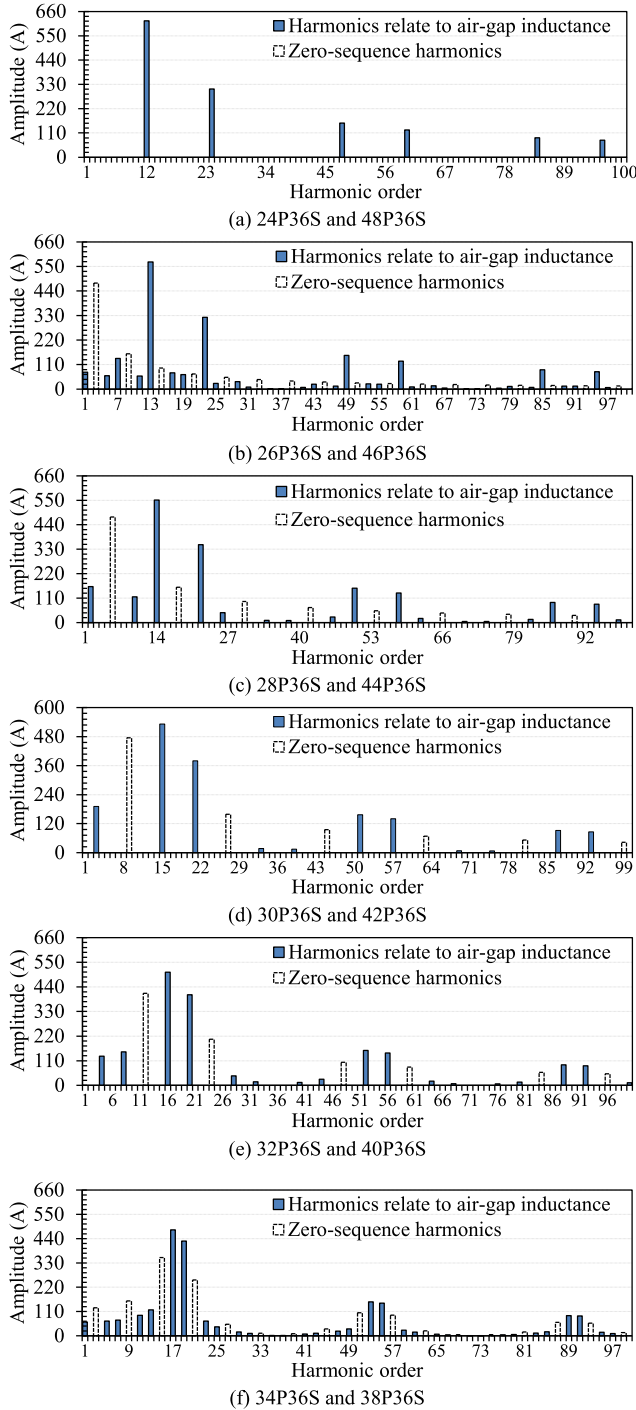
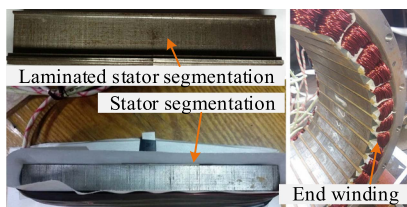Fig. 8.   Spectra of single-phase MMF of FSCWMs.

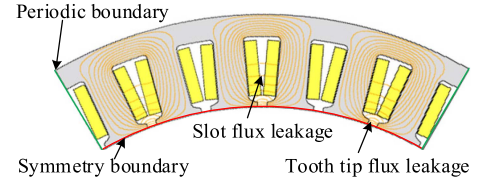Fig. 9.   Segmented stator structure and tooth-wound coil.

Fig. 10.   Boundary conditions in the 2D-FEM model of 30P36S and the calculated stator flux leakage.
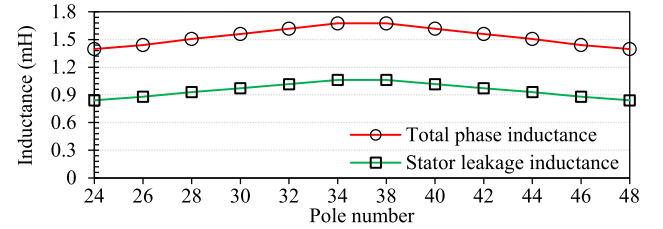

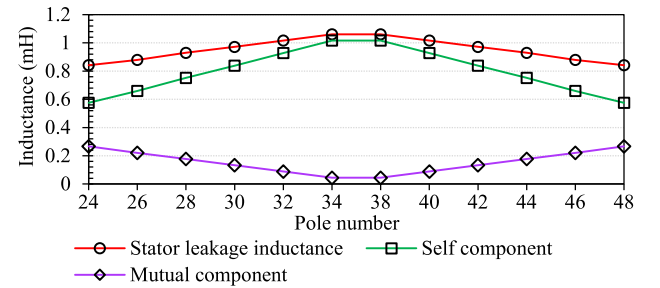Fig. 11.   Stator leakage inductances and phase inductances.

Fig. 12.   Stator leakage inductances and their self- and mutual components.

L_σ can be further separated into the self-component $L_{\sigma s}$ and mutual component $L_{\sigma m}$ by exciting only one phase winding in the FEM model, as (12). Fig. 12 gives the variation of L_σ, $L_{\sigma s}$, and $L_{\sigma m}$. $L_{\sigma s}$ shows the same variation trend as L_σ, in close pole-slot combinations, it has the maximal values. However, the opposite variation is observed for $L_{\sigma m}$, as the close pole-slot combinations have minimal values. Compared to 24P36S, $L_{\sigma m}$ of 34P36S decreases from 0.27mH to 0.04mH, about 1/2 and 1/23 of $L_{\sigma m}$ respectively. Moreover, unlike that for L_g, the mutual coupling factor 1/2 between two phases does not work for correlating $L_{\sigma m}$ and $L_{\sigma s}$. In addition, since L_σ contributes a large portion of L_p in FSCWMs, the mutual component of L_p is also not half of the self-component as well.

$$L_\sigma = L_{\sigma s} + L_{\sigma m} \tag{12}$$

Generally speaking, machines with large $L_{\sigma s}$ and small $L_{\sigma m}$ are preferred when improving fault-tolerant ability, hence close pole-slot combinations, such as 34P36S and 38P36S, are the most competitive candidates.

As for L_{s0}, its variation against pole numbers is similar to that of L_σ, the difference is that L_{s0} varies more sharply, as shown in Fig. 13. The variation trend of L_{s0} can be viewed intuitively from the stray zero-sequence flux linkage ψ_{s0}, as shown in Fig. 14. The amplitude of ψ_{s0} of 34P36S and 38P36S are larger than that in other combinations. As a consequence, in 24P36S and 48P36S, L_{s0} is 0.04mH, only 4.88% of L_σ. Whereas in close
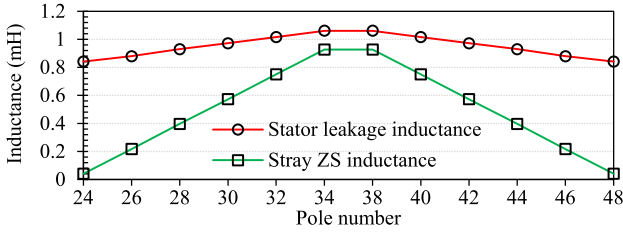
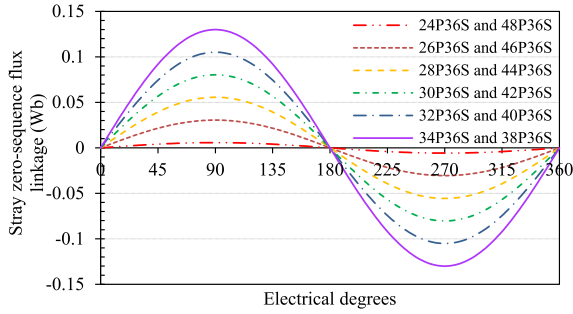Fig. 13. Stator leakage inductances and stray ZS inductances.

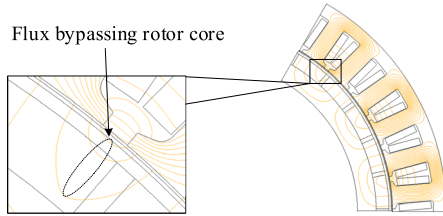Fig. 14. Stray zero-sequence flux linkages of phase winding.

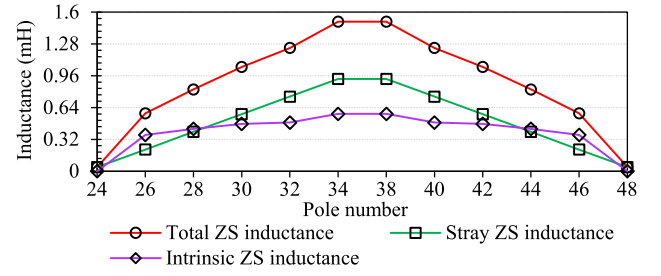Fig. 15. Zero-sequence flux distribution of 30P36S.

Fig. 16. Total ZS inductances and its components.
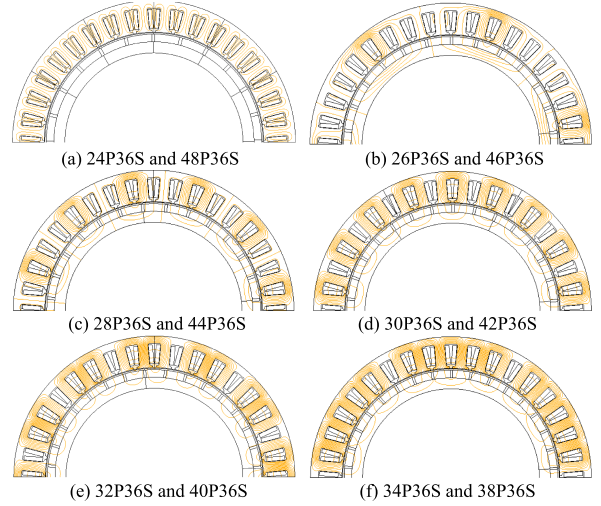
Fig. 17. Contour plots of flux distribution when feeding zero-sequence current and disabling permanent magnets.

pole-slot combinations 34P36S and 38P36S, L_{s0} increases to 0.93mH, nearly 87.4% of L_{σ}.

From the above analysis, it can be concluded that the close pole-slot combinations have the maximal stray ZS inductance, which is desirable to suppress zero-sequence current.

B. Comparison of Stray and Intrinsic ZS Inductances

Analytical calculation (8) of the intrinsic ZS inductance L_{i0} using winding function assumes that all air-gap flux enters the rotor core, and then returns to the stator core by crossing the air gap again. Meanwhile, it assumes that the slot opening $s_o = 0$. These assumptions cause a minor error if the equivalent air gap δ is small [28]. However, for FSCWMs with an SPM rotor, δ is large, and not all air-gap flux flow radially into the rotor core. Part of the flux bypasses the rotor core and returns to the stator side through the air gap directly, as shown in Fig. 15. As a result, the winding function method (8) overestimates the length of the air-gap flux's flowing path, and calculated L_{i0} is smaller than the real value. Hence, to improve the accuracy, L_{i0} is recalculated here by subtracting L_{s0} from the total ZS inductance L_0 from 2D-FEM, as in (13).

$$L_{i0} = L_0 - L_{s0} \quad (13)$$

Fig. 16 shows the variation of L_0, L_{s0}, and L_{i0} against pole numbers. It can be seen that, after considering the true path of zero-sequence flux by FEM, L_{i0} also has maximal values in close pole-slot combinations. Moreover, L_{s0} is larger than L_{i0} in the close pole-slot combinations, such as 32P36S, 34P36S, 38P36S, and 40P36S. Whereas in 26P36S and 46P36S that have obvious distinctions between their pole and slot numbers, L_{s0} is smaller than L_{i0}, and L_0 is dominated by L_{i0}. In addition, it is noteworthy that 24P36S and 48P36S evolved from the 2P3S and 4P3S have extremely low L_0, which should be avoided when requiring a small zero-sequence current.

The variation of L_0, L_{s0}, and L_{i0} can be seen intuitively from the zero-sequence flux distribution, as illustrated in Fig. 17, where the number of flux lines evaluates the total flux quantity. When $2p < z$, the zero-sequence flux induced by a fixed i_0 increases gradually with pole number. Whereas, in the case of $2p > z$, the zero-sequence flux decreases, indicating that in close pole-slot combinations, the zero-sequence flux and L_0 obtain the maximal values. In addition, the portion of zero-sequence flux flowing into the air gap decreases with pole number when $2p < z$, but the zero-sequence flux leakage in the stator increases greatly. This validates the incremental percentage of L_{s0} in L_0.

Fig. 18. Prototypes manufactured and the LCR meter. (a) Serial connection (b) Parallel connection.
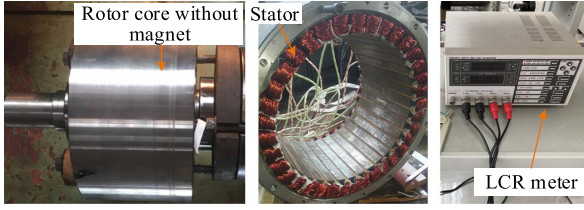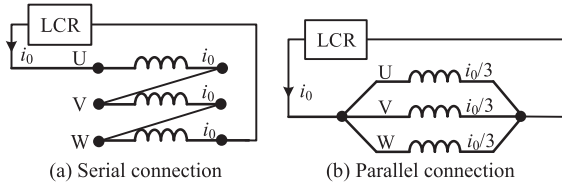

(a) Serial connection   (b) Parallel connection

Fig. 19. Winding connection pattern of Zero-sequence inductance measurement.

Fig. 20. Calculated and measured ZS inductances with and without rotor core.

TABLE II
CALCULATED AND MEASURED TOTAL ZS INDUCTANCE

Machines	24P36S/ 48P36S	26P36S/ 46P36S	28P36S/ 44P36S	30P36S/ 42P36S	32P36S/ 40P36S	34P36S/ 38P36S
L_0 (mH, FEM)	0.06	0.60	0.84	1.06	1.25	1.52
L_0 (mH, Meas)	0.07	0.61	0.85	1.07	1.25	1.53
Error (%)	14.28	1.64	1.18	0.55	0.89	0.65

V. MEASUREMENT AND VALIDATION OF THE VARIATION REGULARITY

Prototypes of the 36-slot stator and rotor core are built to validate the regularities by experiments, as shown in Fig. 18. The surfaced-mounted permanent magnets are not installed on the rotor core, according to model settings in FEM. In this case, the magnetic saturation caused by permanent magnets is avoided. In the stator prototype, coils are wound on each tooth and for the ease of changing winding layouts, each coil has two individual terminals. Once the measurements of a combination are finished, the winding layout can be changed simply by reconnecting coil terminals according to Fig. 6. Another merit is that using the same stator eliminates potential errors from fabrication/assembly tolerance and magnetic property deviation of various prototypes.

A HIOKI 3511-50 LCR meter is used to measure the total ZS inductance L_0. Ideally, the 3-phase windings can be connected either in series or in parallel, as shown in Fig. 19. However, to avoid potential measurement errors caused by the uneven distribution of i_0 due to phase resistance difference, the serial connection pattern is utilized here.

Table II lists the calculated (including the end winding inductance using 3D-FEM) and measured L_0 for all machines. It can be seen that the calculated and measured L_0 show high consistency, and the maximum error is 1.64%. Exceptions are 24P36S and 48P36S, since they have extremely small L_0, the excess inductance of the connecting lines leads to a large error between the calculated and measured results. Nevertheless, the
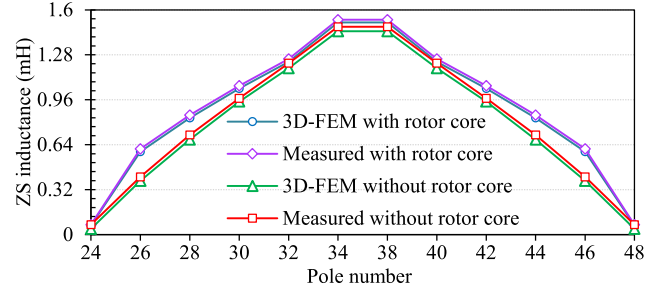
relatively large error in 24P36S and 48P36S do not influence the variation trend of L_0, and the experimentally revealed variation regularity of L_0 is consistent with the calculated one. In addition, the experimental results validate that in close pole-slot combinations, L_0 has maximal values, which help to reduce the zero-sequence current.

For the stray ZS inductance L_{s0}, excluding air-gap flux by imposing constraint conditions like that in the FEM model is impossible in experiments. As a consequence, measuring L_{s0} and then separating L_0 is difficult, if not impossible. The method separating stator leakage inductance is proposed in the standard IEEE 115-2009 using the removed rotor test and search coil. However, this method is practical for ISDWMs but shows low accuracy in FSCWMs due to rich MMF harmonic [24]. So far, there is no practical method to measure L_{s0} of FSCWMs, with acceptable accuracy. Thus, the variation regularity of L_{s0} is indirectly validated here, by measuring ZS inductance with the rotor core removed.

Fig. 20 presents the calculated and measured ZS inductance with and without rotor core, where 3D-FEM is used to account for the end winding inductance and local magnetic saturation. It deserves to note that the LCR meter produces a small current excitation into the phase windings for inductance measurement. Though the current has a minor influence on the saturation level of the stator core, to eliminate the effect of potential magnetic saturation and for a fair comparison, the winding current in the FEM model is set to that output from the LCR meter, i.e., the calculated and measured ZS inductances are derived with identical current excitation.

It can be seen from Fig. 20 that the calculated and measured ZS inductances show good agreement no matter when with and without the rotor core, and the maximum difference is 2.6%. Meanwhile, the variation trend of measured ZS inductances is consistent with the calculated one, verifying that the close pole-slot combinations have the maximal L_{s0}.

In addition, comparing the experimental results with and without the rotor core, the presence of the rotor core increases ZS inductance greatly in 26P36S (46P36S) and 28P36S (44P36S). This can be observed intuitively from Fig. 17(b) and (c) as a large amount of zero-sequence flux flows through the rotor core. Whereas in the close pole-slot combinations, such as 34P36S and 38P36S, the inductance increments are smaller. The reason is that L_{s0} is dominant in these combinations, which are less affected by the rotor core. In addition, this also indicates that

when a large L_0 is required to suppress zero-sequence current, increasing L_{s0} will be more effective than L_{i0}.

VI. CONCLUSION

To mitigate the zero-sequence current and its influence, ZS inductance must be carefully designed. This paper reveals the variation regularities of ZS inductance, its components, and other inductances, and the findings help to select optimal pole/slot combinations at the machine design stage.

The experimental measurements on the 36-slot prototypes have validated these regularities. More importantly, similar variation regularities are found in the calculated inductance of 54-slots and 81-slots FSCWMs with different pole numbers, demonstrating that the regularities derived are independent of specific slot numbers. These regularities help to determine the optimal pole/slot combinations and solve problems caused by the zero-sequence current at the machine's design stage.

REFERENCES

[1] H. Vansompel and P. Sergeant, "Extended end-winding cooling insert for high power density electric machines with concentrated windings," *IEEE Trans. Energy Convers.*, vol. 35, no. 2, pp. 948–955, Jun. 2020.

[2] A. Tessarolo, F. Luise, S. Pieri, A. Benedetti, M. Bortolozzi, and M. De Martin, "Design for manufacturability of an off-shore direct-drive wind generator: An insight into additional loss prediction and mitigation," *IEEE Trans. Ind. Appl.*, vol. 53, no. 5, pp. 4831–4842, Sep./Oct. 2017.

[3] S. Zhu, J. Ji, W. Zhao, J. Zheng, Y. Mao, and G. Liu, "Unequal teeth design to reduce electromagnetic vibration in fractional-slot concentrated-windings permanent-magnet machine," *J. Magn.*, vol. 24, no. 4, pp. 657–667, Dec. 2019.

[4] A. E. Hoffer, I. Petrov, J. J. Pyrhönen, J. A. Tapia, and G. Bramerdorfer, "Analysis of a tooth-coil winding permanent-magnet synchronous machine with an unequal teeth width," *IEEE Access*, vol. 8, pp. 71512–71524, 2020.

[5] J. Cros and P. Viarouge, "Synthesis of high performance PM motors with concentrated windings," *IEEE Trans. Energy Convers.*, vol. 17, no. 2, pp. 248–253, Jun. 2002.

[6] K. Wang, Z. Q. Zhu, and G. Ombach, "Synthesis of high performance fractional-slot permanent-magnet machines with coil-pitch of two slot-pitches," *IEEE Trans. Energy Convers.*, vol. 29, no. 3, pp. 758–770, Sep. 2014.

[7] A. Tessarolo, "A quadratic-programming approach to the design optimization of fractional-slot concentrated windings for surface permanent-magnet machines," *IEEE Trans. Energy Convers.*, vol. 33, no. 1, pp. 442–452, Mar. 2018.

[8] A. Tessarolo, C. Ciriani, N. Elloumi, and M. Mezzarobba, "Potentials and limits of three-phase fractional-slot concentrated winding optimization," in *Proc. IEEE Workshop Elect. Machines Des., Control Diagnosis*, 2021, pp. 143–148.

[9] E. Carraro, N. Bianchi, S. Zhang, and M. Koch, "Design and performance comparison of fractional slot concentrated winding spoke type synchronous motors with different slot-pole combinations," *IEEE Trans. Ind. Appl.*, vol. 54, no. 3, pp. 2276–2284, May/Jun. 2018.

[10] A. Tessarolo, C. Ciriani, M. Bortolozzi, M. Mezzarobba, and N. Barbini, "Investigation into multi-layer fractional-slot concentrated windings with unconventional slot-pole combinations," *IEEE Trans. Energy Convers.*, vol. 34, no. 4, pp. 1985–1996, Dec. 2019.

[11] I. Petrov, C. Di, P. Lindh, M. Niemelä, A.-K. Repo, and J. Pyrhönen, "Fault-tolerant modular stator concentrated winding permanent magnet machine," *IEEE Access*, vol. 8, pp. 7806–7816, 2020.

[12] Y. Fan, C. Li, W. Zhu, X. Zhang, L. Zhang, and M. Cheng, "Stator winding interturn short-circuit faults severity detection controlled by OW-SVPWM without CMV of a five-phase FTFSCW-IPM," *IEEE Trans. Ind. Appl.*, vol. 53, no. 1, pp. 194–202, Jan./Feb. 2017.

[13] H. Zhan, Z. Q. Zhu, and M. Odavic, "Nonparametric sensorless drive method for open-winding PMSM based on zero-sequence back EMF with circulating current suppression," *IEEE Trans. Power Electron.*, vol. 32, no. 5, pp. 3808–3817, May 2017.

[14] Y. Guo, L. Wu, X. Huang, Y. Fang, and J. Liu, "Adaptive torque ripple suppression methods of three-phase PMSM during single-phase open-circuit fault-tolerant operation," *IEEE Trans. Ind. Appl.*, vol. 56, no. 5, pp. 4955–4965, Sep./Oct. 2020.

[15] T. Hackner, J. Pforr, H. Polinder, and J. A. Ferreira, "Optimization of the winding arrangement to increase the zero-sequence inductance of a synchronous machine with multifunctional converter drive," *IEEE Trans. Ind. Appl.*, vol. 48, no. 6, pp. 2277–2286, Nov./Dec. 2012.

[16] L. D. Sousa and H. Dogan, "Method of evaluating the zero-sequence inductance ratio for electrical machines," in *Proc. 14th Eur. Conf. Power Electron. Appl.*, 2011, pp. 1–10.

[17] S. Chevailler, L. Feng, and A. Binder, "Short-circuit faults in distributed and concentrated windings of PM synchronous motors," in *Proc. Eur. Conf. Power Electron. Appl.*, 2007, pp. 1–10.

[18] L. Rovere, A. Formentini, G. L. Calzo, P. Zanchetta, and T. Cox, "Zero-sequence voltage elimination for dual-fed common DC-link open-end winding PMSM high-speed starter–generator—Part I: Modulation," *IEEE Trans. Ind. Appl.*, vol. 55, no. 6, pp. 7804–7812, Nov./Dec. 2019.

[19] J. Shim, H. Choi, and J.-I. Ha, "Zero-sequence current suppression with dead-time compensation control in open-end winding PMSM," in *Proc. IEEE Energy Convers. Congr. Expo.*, 2020, pp. 3051–3056.

[20] L. Alberti and N. Bianchi, "Theory and design of fractional-slot multilayer windings," *IEEE Trans. Ind. Appl.*, vol. 49, no. 2, pp. 841–849, Mar./Apr. 2013.

[21] E. Fornasiero, L. Alberti, N. Bianchi, and S. Bolognani, "Considerations on selecting fractional-slot nonoverlapped coil windings," *IEEE Trans. Ind. Appl.*, vol. 49, no. 3, pp. 1316–1324, May/Jun. 2013.

[22] N. Bianchi, S. Bolognani, M. D. Pre, and G. Grezzani, "Design considerations for fractional-slot winding configurations of synchronous machines," *IEEE Trans. Ind. Appl.*, vol. 42, no. 4, pp. 997–1006, Jul./Aug. 2006.

[23] W. Chengyu, L. Chuang, J. Renhua, Z. Jie, and N. Yinhang, "Effect of slot-and-pole combination on the flux-weakening properties of fractional-slot concentrated windings," in *Proc. 17th Int. Conf. Elect. Machines Syst.*, 2014, pp. 344–348.

[24] C. M. Donaghy-Spargo, B. C. Mecrow, and J. D. Widmer, "On the influence of increased stator leakage inductance in single-tooth wound synchronous reluctance motors," *IEEE Trans. Ind. Electron.*, vol. 65, no. 6, pp. 4475–4482, Jun. 2018.

[25] W. M. Arshad, H. Lendenmann, and H. Persson, "End-winding inductances of MVA machines through FEM computations and IEC-specified measurements," *IEEE Trans. Ind. Appl.*, vol. 44, no. 6, pp. 1693–1700, Nov./Dec. 2008.

[26] O. Chiver, E. Micu, and C. Barz, "Stator winding leakage inductances determination using finite elements method," in *Proc. 11th Int. Conf. Optim. Elect. Electron. Equip.*, 2008, pp. 69–74.

[27] A. T. Brahimi, A. Foggia, and G. Meunier, "End winding reactance computation using a 3D finite element program," *IEEE Trans. Magn.*, vol. 29, no. 2, pp. 1411–1414, Mar. 1993.

[28] A. Tessarolo, "Accurate computation of multiphase synchronous machine inductances based on winding function theory," *IEEE Trans. Energy Convers.*, vol. 27, no. 4, pp. 895–904, Dec. 2012.

Zichong Zhu received the Ph.D. degree in electrical engineering from Southeast University, Nanjing, China, in 2021. After graduation, he joined Nanjing Tech University, Nanjing, as a Lecturer. His research interests include the electromagnetic analysis, thermal management, optimization and control of permanent magnet synchronous machines for the wheel-hub propulsion, gas compression, fly-wheel energy storage, and servo applications.

Jun Deng received the B.S. degree in 2021 from the Taizhou Institute of Science and Technology, Nanjing, China. He is currently working toward the M.S. degree with the College of Electrical Engineering and Control Science, Nanjing Tech University, Nanjing. His main research interests include the design and multiphysic optimization of high-speed permanent magnet synchronous motors.

Xun Dou (Member, IEEE) received the B.S., M.S., and Ph.D. degrees from Southeast University, Nanjing, China, in 2001, 2004, and 2012, respectively. She is currently an Associate Professor with Nanjing Tech University, Nanjing. From 2015 to 2016, she was a Visiting Scholar with the School of Mechanical Engineering, University of California, Los Angeles, Los Angeles, CA, USA. She is the author of more than 20 articles, and more than ten inventions. Her research interests include integrated energy systems, power markets and power economics, demand response, and power planning.

Yunkai Huang received the M.Sc. and Ph.D. degrees in electrical engineering from Southeast University, Nanjing, China, in 2001 and 2007, respectively. He is currently a Professor with the School of Electrical Engineering, Southeast University. His research interests include design and control of PM machines, particularly the high-speed brushless machine, applications in domestic appliances, electric vehicles, and wind power generation systems.

Lei Mei (Member, IEEE) received the B.S. degree in automation from East China Shipbuilding Institute, Zhenjiang, China, in 2000, and the Ph.D. degree in electrical engineering from the Nanjing University of Aeronautics and Astronautics, Nanjing, China, in 2009. In 2009, he joined the Department of Electrical Engineering, Nanjing Tech University, Nanjing, where he is currently an Associate Professor with the College of Electrical Engineering and Control Science. His research interests include magnetic bearings and special electrical machines.

Jianning Dong (Member, IEEE) received the B.S. and Ph.D. degrees in electrical engineering from Southeast University, Nanjing, China, in 2010 and 2015, respectively. Since 2016, he has been an Assistant Professor with the Delft University of Technology (TU Delft), Delft, The Netherlands. Before joining TU Delft, he was a Postdoctoral Researcher with McMaster Automotive Resource Centre, McMaster University, Hamilton, ON, Canada. His main research interests include design, modeling, and control of electromechanical systems.